ALL-SILICON TANDEM CELLS BASED ON "ARTIFICIAL" SEMICONDUCTOR SYNTHESISED USING SILICON QUANTUM DOTS IN A DIELECTRIC MATRIX

Green, M.A., Cho, E.-C., Cho, Y., Huang, Y., Pink, E., Trupke, T., Lin, A.,
Fangsuwannarak, T., Puzzer, T., Conibeer, G. and Corkish, R.
Centre of Excellence for Advanced Silicon Photovoltaics and Photonics
University of New South Wales, Sydney, Australia, 2052
Phone: +(61-2) 9385-4018 Fax: +(61-2) 9662-4240
Email: m.green@unsw.edu.au

ABSTRACT: To reach its most competitive long-term position, photovoltaics must push towards ever-increasing energy conversion efficiency while retaining low areal production costs. The most developed approach for improving this efficiency beyond that of a standard cell is to use a tandem stack of cells, with each cell in the stack having a different bandgap. Our group is exploring the use of nanostructural engineering to control silicon's bandgap in quantum-confined structures to develop such tandem stacks based entirely on crystalline silicon and its compounds with oxygen, nitrogen and carbon. Recent experimental and theoretical progress is outlined as are the main challenges for future work.
Keywords: Si-Films, Tandem, Quantum Well

1. INTRODUCTION

To reach its most competitive long-term position, it has been argued that photovoltaics must push towards ever-increasing energy conversion efficiency while retaining low areal processing costs [1]. The most developed approach for improving efficiency above that of a standard cell is to use tandem stacks of cells of different bandgap. Tandem stacks based entirely on crystalline silicon and its compounds with oxygen, nitrogen and carbon would have many attractions, as they would retain the strengths of silicon technology (durability, non-toxicity, material abundance), while giving the design flexibility offered by otherwise less attractive material systems.

Two strategies for implementing tandem cells can be identified in past work. One, the most successful to date, is based on the fortuitous availability of semiconductor material with the required complementary properties. GaInP/GaAs/Ge technology falls into this category as does the "micromorph" a-Si/μc-Si tandem. The second strategy encompasses a generic approach which allows the progressive control of bandgap by changing processing conditions. Alloying is one approach for such control, such as in a-Si:Ge based tandem cells. Quantum confinement, where the bandgap is controlled by the lateral dimensions of the active material, is another. A generic approach may be essential for implementing tandem stacks involving large numbers of cells. Although increasing spectral sensitivity makes stacks with 10 or more cells an unlikely proposition [2], stacks involving 5-6 cells could well be of interest in the long-term.

2. CONCEPT

By restricting at least one dimension of silicon to the nanoregime (10 nm or less), silicon's effective band-gap is increased. Our early experiments involved carefully thinning the already quite thin silicon layer (50 nm thick) in commercially available silicon-on-insulator wafers [3]. For possibly the first time, clear evidence for quantum-confined bandgap increase was demonstrated from photoluminescence measurements on such devices, with bandgap up to 1.7 eV measured for layers about 1 nm thick [3]. Importantly, the strength of the optical processes initially increased as the layer was thinned, as expected on fundamental grounds, but providing an added bonus for solar applications.

Approaches explored for producing such 2D confined material in a low-cost way did not prove particularly encouraging. However, an approach by Zacharias et al. [4] based on producing 0D silicon quantum dots by depositing alternating layers of stoichiometric oxide followed by silicon-rich oxide appears more promising (Fig. 1). On heating, silicon precipitates from the silicon-rich layers as approximately spherical quantum dots of a diameter close to the original layer thickness. Hence, control of the diameter and one spatial co-ordinate of the dots is possible. The dots precipitate more or less uniformly in the other 2 spatial directions, as expected from phase separation theories [5]. It is possible to form dots that are separated by a distance of the same order of magnitude as the dot diameter, giving prospects for wave-function overlap between dots and hence for electron transfer between them.

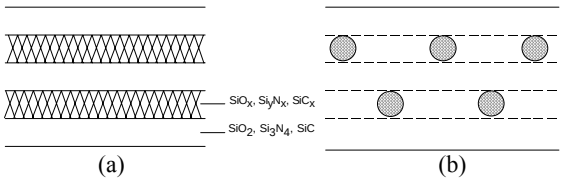

Figure 1: (a) Precursor stoichiometric and non-stoichiometric, silicon-rich layers for forming silicon quantum dots; (b) precipitation of dots within the silicon-rich layers.

Dots have the advantage of lower surface area compared to 2D layers (once dots are separated by about half their radius) and of being single crystalline (no grain boundaries since smaller than a grain!). Doping of dots has also been demonstrated in both our work and earlier work using different preparation techniques [6]. Doping is expected to allow the same control over material work-function and electron-hole concentrations as in bulk semiconductors [7].

Figure 2 shows QD material prepared in the previous way while Fig. 3 shows a possible 3-cell tandem cell design based on the present concept. The bottom cell is a thin-film, unconfined polycrystalline silicon cell with properties similar to those demonstrated by the

"crystalline silicon on glass" cells of CSG Solar [8]. The middle cell is a quantum dot cell, with the quantum dot diameter relatively large, chosen to give a bandgap of about 1.5 eV. It is connected to the bottom cell by a "tunnelling" or more probably, a defect dominated, high recombination junction. The material in the inter-connection region could be quantum dot material, but employ smaller dots than the overlying region.

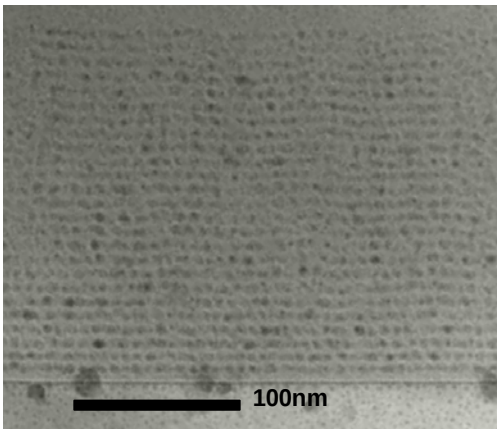

Figure 2: TEM image of quantum dot material synthesised using the approach of Fig. 1.

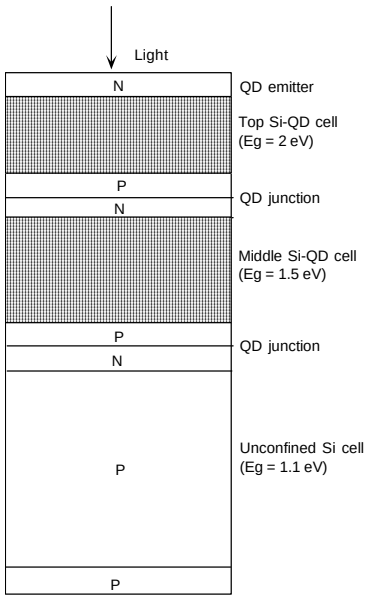

Figure 3: All-silicon 3-cell tandem stack based on silicon quantum dots.

A third cell is also shown at the top in Fig. 3. This would have smaller QD size than that in the cell underlying it to give a bandgap of about 2.0 eV. With the selected bandgaps, each cell could, in practice, generate 10 mA/cm^2 in bright sunlight, allowing current matching. Upper QD cells are likely to be more strongly absorbing than the unconstrained cell due to the effects of confinement, with the required thickness for these cells estimated as of the order of 100 nm.

In principle, fabrication processes could parallel those used for CSG technology, with all layers deposited in the amorphous phase and subsequently crystallised during thermal treatments. The high-density contacting scheme used by CSG Solar would be ideal for this structure (Fig. 4). The lower current density should help avoid the need for TCO (transparent conducting oxide) layers also in this case, saving cost and eliminating documented durability issues [9,10].

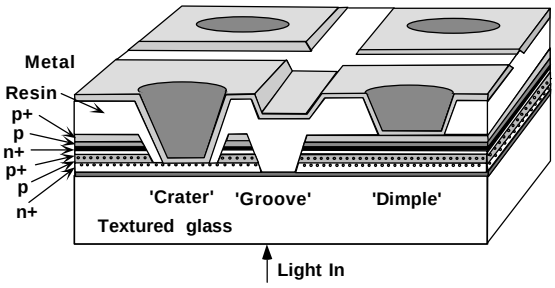

Figure 4: CSG solar cell with quantum dots.

The challenges in implementing such technology are far from trivial but progress to date has been promising.

3. OPTICAL PROPERTIES

3.1 Experimental

Figure 5 shows measured room-temperature photoluminescence (PL) spectrum from silicon quantum dots such as shown n Fig. 2. The peak of the PL signal shifts to higher energies as the dot size decreases, due to confinement in the silicon material as expected. The strength of the emission also initially increases, as would be expected as a result of confinement. The broadness of the peak is attributed to the range of dot sizes formed by the process. This size range tends to become larger for large dots. While the growth of small dots may be controlled by 2D growth mechanisms, the thicker layers used for the larger dots may allow 3D growth.

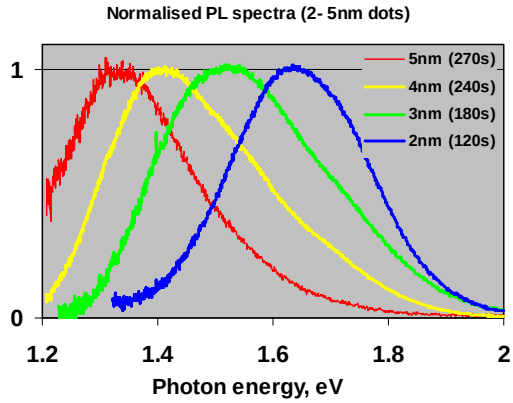

Figure 5: RT photoluminescence from QD material with dots of different nominal diameter.

3.2 Theoretical Issues

One early concern was that confinement ideally produces discrete states above the bandgap that may restrict absorption to narrow photon energy bands rather than the broadband absorption desirable for solar applications. For confinement in one direction, the confined energies are given by the following equation:

$$E = \frac{\hbar^2 \chi_{nl}^2}{2m^* a^2} \qquad (1)$$

where $\hbar$ is the reduced Planck constant, a is the thickness of the confined dimension and χ_{nl} is the argument giving the *nth* zero of the zero order spherical Bessel function (lower case j-function). These arguments equal $n\pi$. Hence, allowed states increase as the square of the quantum number, n and there is a large energy gap between the first and higher energy states (Fig. 6).

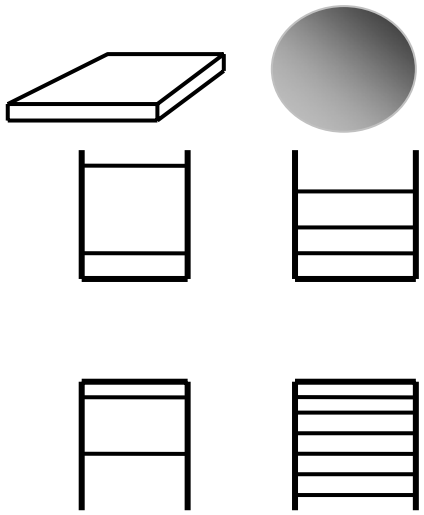

Figure 6: Comparison of solutions for confined energies for 1D and 3D confinement.

However, 3D confinement introduces additional energy solutions. In the simplest case (spherical dot with isotropic effective mass m^* and infinite barriers), the confined energies are also given by Eq. (1) where a is now the dot radius [11]. χ_{nl} in this case is the *nth* zero of the spherical Bessel function of order l, with all values of l allowed.

Going from confinement in 1D to 3D therefore greatly increases the number of confined states, since there are an infinite number of spherical Bessel functions of other than zero order (only those of zero, first and second order have their first zero smaller than 2π, however). These additional solutions are associated with different angular momentum, with optical transitions allowed between states of the same value of l. Since silicon's indirect transition is essentially forbidden in any case, the distinction between allowed and forbidden transitions is not as important as in direct bandgap material.

Incorporating silicon's anisotropic CB (conduction band) effective mass eliminates some of the degeneracies in the isotropic solution. Three quantum numbers are required to describe states in silicon's CB in this case, with the increased number of states further reducing the energy separation between states (Fig. 7). The double degeneracy of the valence band (light and heavy holes) and the close proximity of the split-off band in silicon complicates the treatment of the valence band severely [12].

A high density of discrete VB states result (Fig. 7). Interactions between the 6 degenerate conduction band valleys also splits the degeneracies associated with the CB [12]. Proximity to other dots causes additional splitting of allowed states causing each level in Fig. 7 to broaden into a band of width determined by the dot spacing. Variations in the dot diameter between dots will cause additional overlapping of the energies of allowed and non-allowed states. The conclusion is that there will be an essentially continuous distribution of optical transition energies allowed to electrons to the conduction from the valence bands of QD material, with the band edges determined by the diameter of the largest dots in this material. The photoluminescence results of Fig. 5 support this view.

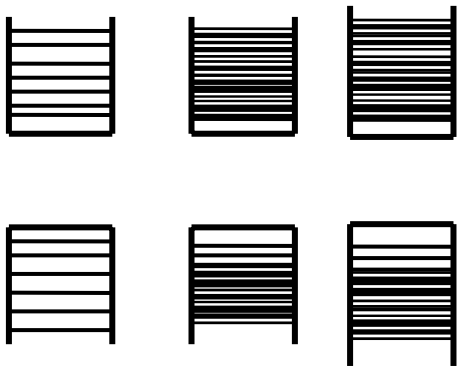

Figure 7: Effect of silicon's anisotropic CB mass (left), interaction between the bands (centre) and dot size increase of 10% (right) on available energy states.

4. TRANSPORT PROPERTIES

4.1 Theoretical Framework

The wavefunction of an electron confined to a spherical dot penetrates into the surrounding material, decaying approximately as $exp\ (-r/L_d)/r$ where r is the distance from the centre of the dot. The decay length L_d is determined by the barrier height imposed by the material in which the dot is embedded, with the case of carbide, nitride and oxide matrices shown in Fig. 8. In the simplest case, the decay length is given by:

$$L_d = 1/\sqrt{2m^{**}(V_o - E_n)} = 0.1952nm/\sqrt{\frac{m^{**}\Delta E}{m_o}} \qquad (2)$$

The latter expression holds when ΔE, the difference between the CB edge of the matrix and the confined energy level, is in *eV*. m^{**} is the effective mass in the matrix material.

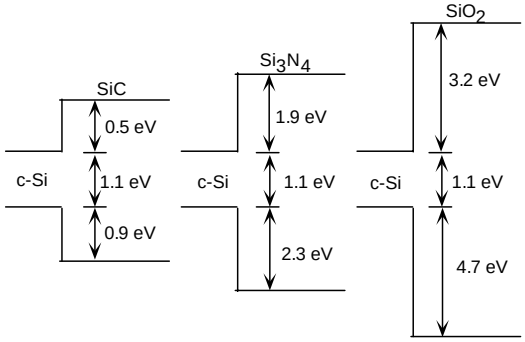

Figure 8: Indicative bulk band alignments between crystalline silicon and its carbide, nitride and oxide.

Although the wave function decays rapidly, measurable current between dots is predicted for dot spacing comparable to tunnelling thicknesses (e.g., below 3 nm for the oxide case, with higher values for the other cases).

Idealised or Bloch carrier mobility in the quantum dot material can be calculated by first calculating the band structure of the idealised quantum dot material, using techniques similar to those for bulk semi-conductors, and then finding the corresponding effective mass at the band edge. Given a carrier scattering time τ, mobility is calculated as:

$$\mu = q\tau / m^*_{QD} \qquad (3)$$

Using the band structure calculation approach described elsewhere [13], approximating the quantum dot shape as cubic, assuming $\tau = 30$ fs and that the effective mass in the matrix material equals that in the silicon, gives the mobility values of Fig. 9.

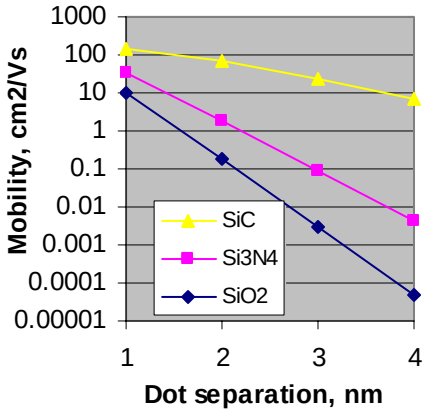

Figure 9: Bloch mobility in QD material versus distance between dots (2 nm cubic dot).

These results suggest that dots in an SiO_2 matrix would have to be spaced no further than 1-2 nm apart, while they could be separated by more than 4 nm in SiC. The same type of calculation allows the effect of fluctuations in spacing and size of the dots to be investigated. It is found that the calculated Bloch mobilities do not depend strongly on variations in the dot spacing but do depend strongly on dot size within the QD material. This arises since the formulation does not incorporate phonons and therefore consider only transitions that are energy conserving, at least Planckian timescales.

Much higher conductivity is measured experimentally than calculated for dots in an oxide matrix with the experimentally observed spacings and dot size fluctuations.

This suggests not only phonons, but also that defects in the matrix material may be involved in the transport process. Even in high quality oxides, measurable leakage currents can flow and are usually attributed to hopping through defect states in the oxide lying at energies close to the band edge (Fig. 10).

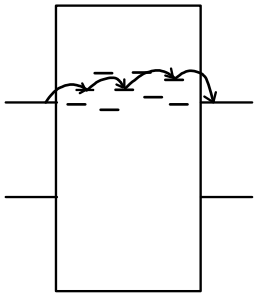

Figure 10: Hopping transport in high quality oxide.

Our calculations show a likely enhancement of this effect in QD material due to a process similar to resonant tunnelling through defect states. If the energy level associated with the defect lies close in energy to the confined bandgap edge in the dot (Fig. 11), the conditions for resonance are ideal. It follows that, if a defect of the resonant energy lies anywhere on the transport path between dots, it will automatically be selected from the defect pool and resonantly enhance current flow. Calculations show that the resulting mobility is not strongly dependent on the spatial position of the defect on this transport path, relative to the dot positions.

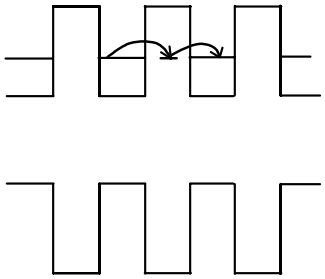

Figure 11: Resonant enhancement of transport when defects are present in the matrix.

Figure 12 shows the calculated boost in mobility assuming a monolayer of defects between quantum dots (in this case, an electron would see at least one defect at the resonant energy regardless of the direction in which it propagates between dots). Lower defect densities would give proportionately intermediate results.

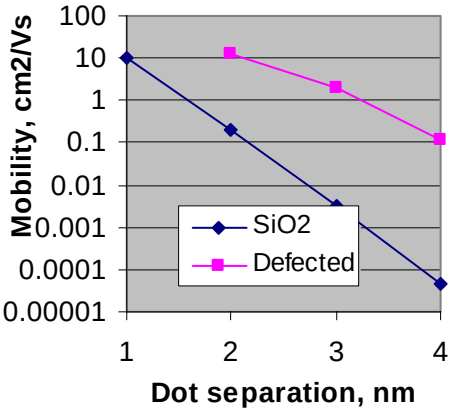

Figure 12: Bloch mobility for an oxide matrix in the presence of a monolayer of reasonantly positioned defects.

Transport between the ground state energy of small dots and excited states of larger dots is possible, although selection rules apply if these transitions are direct. Phonon involvement will relax these rules, as well as allowing transitions from the larger to the smaller dot. Without phonon involvement, a small dot between two large dots would not participate in transport between the ground states of the large dots. The transport distance between the large dots, however, would be reduced by discounting any portion of it passing through a small dot.

As a consequence of the above, phonons and defects are therefore expected to play a large role in determining mobility in the matrix material.

4.2 Experimental Conductivity

Figure 13 shows the measured resistivity of our QD material as a function of temperature, as well as the associated thermal activation energy [14]. Resistivity for this sample is about 200Ωcm at room temperature, increasing as temperature decreases. The activation energy is in the 10-20 meV range at all but low temperature. This corresponds to energies where there are high densities of states for TA phonons in bulk silicon. The confined phonon density-of-states spectra do not deviate significantly from that of bulk silicon as dot size deceases [15].

Present work involves a systematic investigation of conductivity versus preparation conditions in undoped and doped material in oxide and nitride matrices. It is planned also to extend these studies to carbide matrices.

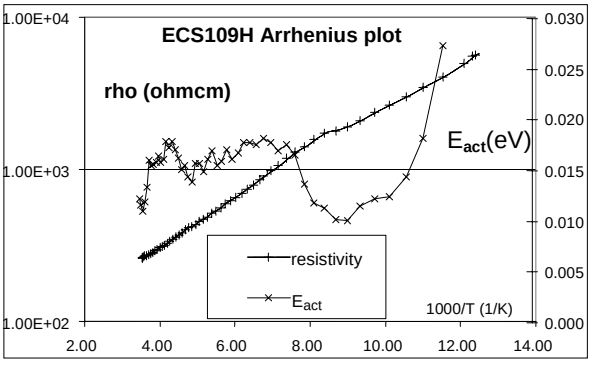

Figure 13: Electrical resistivity and corresponding thermal activation energy of silicon QD material layers in the lateral direction [14].

5. SUMMARY AND CONCLUSIONS

Progress is reported towards implementing tandem cells based entirely on silicon by using quantum confinement. Physically, control of quantum dot size and density in both oxide and nitride matrices has been demonstrated and high-resolution TEM characterisation approaches developed, although the latter are very labour intensive. The control of bandgap by controlling the size of silicon quantum dots also has been demonstrated using photoluminscence measurements.

Techniques for calculating the electronic band structure of the dots and associated transport properties have been developed and the effects of dot size and spacing, plus the effect of defects in the matrix material, calculated. The measured transport properties of the dots have been encouraging, with defects and phonons postulated to play a major role.

The next goal is to show that the increased bandgaps demonstrated optically can be converted to higher voltage output than from unconfined silicon, the essential requirement for demonstrating improved performance using the tandem approach.

ACKNOWLEDGEMENTS

We gratefully acknowledge the support of the Centre of Excellence for Advanced Silicon Photovoltaics and Photonics by the Australian Research Council under its Research Centres of Excellence Scheme. We also thank other members of the Centre and visitors to it for their contributions to this work.

REFERENCES

[1] M.A. Green, "Third Generation Photovoltaics: Advanced Solar Electricity Generation", (Springer-Verlag, Berlin, 2003).
[2] A.S. Brown and M.A. Green, "Limiting Efficiency for Current-Constrained Two-Terminal Tandem Cell Stacks", Progress in Photovoltaics 10, 299-307 (2002).
[3] E.C. Cho, M.A. Green, J. Xia, R. Corkish, P. Reece and M. Gal, Appl. Phys. Lett. 84, 2286 (2004).
[4] M. Zacharias, J. Heitmann, R. Scholz, U. Kahler, M. Schmidt, and J. Bläsing, Appl. Phys. Lett. 80, 661 (2002).
[5] J.W. Cahn, J. Chem. Phys. 42, 93, 1965.
[6] Fujii et al, J. Appl. Phys. 83, 7953, 1998.
[7] D.V. Melnikov and J.R. Chelikowsky, Phys. Rev. Lett. 92, 46803 (2004).
[8] M.A. Green et al., Solar Energy 77, 857 (2004).
[9] T.J. McMahon, "Accelerated Testing and Failure of Thin-Film PV Modules", Progress in Photovoltaics 12, 235-248 (2004).
[10] E.L. Mayer and E.E. van Dyk, "Assessing the Reliability and Degradation of Photovoltaic Module Performance Parameters", IEEE Trans. on Reliability 53, 83 (2004).
[11] U. Woggon,, Optical Properties of Quantum Dots, Springer, Berlin, 1996.
[12] Y.M. Niquet, C. Delerue, G. Allan and M. Lannoo, Phys. Rev. B62, 5109 (2000).
[13] C.W. Jiang, M.A. Green, R. Corkish and G. Conibeer, "Energy Band Calculations for Si QD Solar Cells", PVSEC-15, Shanghai, October, 2005.
[14] E. Pink, BE thesis, University of New South Wales, 2004.
[15] M.R. Zachariah, M.J. Carrier, E. Blaisten-Barojas, P. Phys. Chem. 100, 14856 (1996).